IEICE TRANS. INF. & SYST., VOL.E100–D, NO.2 FEBRUARY 2017

LETTER

# A Spectrum-Based Saliency Detection Algorithm for Millimeter-Wave InSAR Imaging with Sparse Sensing

**Yilong ZHANG**[†*a)], ***Nonmember***, **Yuehua LI**[†b)], ***Member***, ***and*** **Safieddin SAFAVI-NAEINI**[††c)], ***Nonmember***

**SUMMARY** Object detection in millimeter-wave Interferometric Synthetic Aperture Radiometer (InSAR) imaging is always a crucial task. Facing unpredictable and numerous objects, traditional object detection models running after the InSAR system accomplishing imaging suffer from disadvantages such as complex clutter backgrounds, weak intensity of objects, Gibbs ringing, which makes a general purpose saliency detection system for InSAR necessary. This letter proposes a spectrum-based saliency detection algorithm to extract the salient regions from unknown backgrounds cooperating with sparse sensing InSAR imaging procedure. Directly using the interferometric value and sparse information of scenes in the basis of the Discrete Cosine Transform (DCT) domain adopted by InSAR imaging procedure, the proposed algorithm isolates the support of saliency region and then inversely transforms it back to calculate the saliency map. Comparing with other detecting algorithms which run after accomplishing imaging, the proposed algorithm will not be affected by information-loss accused by imaging procedure. Experimental results prove that it is effective and adaptable for millimeter-wave InSAR imaging.

***key words:*** *millimeter-wave, InSAR, saliency, sparse*

## 1. Introduction

Object detection represents key components of many millimeter-wave interferometric synthetic aperture radiometer (InSAR) imaging applications [1], such as indoor security, aircraft navigation, environment monitoring, satellite remote sensing, etc., as its advantages of all-weather condition, high-resolution, rapid and accurate imaging data collection.

A number of object detection algorithms deriving from optical image processing have been proposed to cope with this issue. Based on natural spatial statistics of objects and background, most detection algorithms require detailed outline information between objects and background or specific classifiers to evaluate many image windows in a sliding window fashion [2].

However, facing unpredictable and numerous objects, due to imaging mechanism of InSAR system measuring the correlation value of scenes directly and then reconstructing images, InSAR images suffer from complex clutter backgrounds, weak intensity of objects, information-loss accused by imaging procedure, Gibbs ringing effect of the edges between objects and background, which easily invalidates natural spatial domain object detection algorithms.

Salient object regions in natural scenes are generally regarded as objects stand out relative to its backgrounds and thus capture immediate attention. Human brain can focus on general salient objects rapidly in a clustered visual scene without training. However, being able to automatically, efficiently, and accurately estimate salient object regions is still challenging and highly desirable in computer vision given the ability to isolate the object from complex clutter backgrounds. It is believed that human visual attention results both from the fast and simple bottom-up pre-attentive saliency detection and slower and complex top-down attention saliency detection. Sharing the same mechanism, there are also two kinds of design methods of saliency detection algorithms in computer vision: bottom-up saliency detection and top-down saliency detection [3]. The latter one needs enough outline information of object and training in order to detect specific object categories, which is easily achieved for optical images but difficult for InSAR images. This letter adopts a bottom-up saliency detection method based on the characteristics of the sparse sensing imaging mechanism of InSAR system.

Directly using the interferometric value and sparse information of scenes in the basis of the DCT domain adopted by InSAR imaging procedure, the proposed algorithm isolates the support of saliency region and then inversely transforms it back to calculate the saliency map.

## 2. Millimeter-Wave InSAR Imaging with Sparse Sensing

In this section, we briefly recall the basic concepts of Millimeter-wave InSAR imaging and establish sparse InSAR imaging model based on DCT.

Millimeter-wave InSAR measures the interferometric correlation value, namely the visibility function, between pairs of spatially separated antennas. The visibility function is defined as:

Manuscript received June 6, 2016.
Manuscript revised August 31, 2016.
Manuscript publicized October 25, 2016.

[†]The authors are with School of Electronic and Optical Engineering, Nanjing University of Science and Technology, Nanjing, China.
[††]The author is with CIARS (the Centre for Intelligent Antenna and Radio Systems), Department of Electrical and Computer Engineering, University of Waterloo, Waterloo, Canada.
[*]Presently, with CIARS, Department of Electrical and Computer Engineering, University of Waterloo, Waterloo, Canada.
a) E-mail: yilong.zhang@uwaterloo.ca
b) E-mail: nlglyh2013@sina.cn (Corresponding author)
c) E-mail: safavi@uwaterloo.ca
DOI: 10.1587/transinf.2016EDL8119

$$V(u,v)=\iint_{\xi^2+\eta^2\le 1} T(\xi,\eta)r\left(-\frac{u\xi+v\eta}{f_0}\right)e^{-j2\pi(u\xi+v\eta)}d\xi d\eta \quad (1)$$

Where $(\xi,\eta)=(\sin\theta\cos\phi,\sin\theta\sin\phi)$ is the polar coordinate with respect to the spatial $x$ and $y$ axes, $f_0$ is the center frequency, and $r\left(-\frac{u\xi+v\eta}{f_0}\right)$ is the fringe washing function. The brightness temperature and the visibility function are related by the Fourier transform in the ideal system condition. For digital signal processing, the radiation source $S$ is dispersed into $N$ small parts. Ignoring the fringe washing function in ideal case, the visibility function can be expressed as:

$$V_{c,l}=\sum_{n=1}^{N} T(x_n,y_n)e^{-jK(R_n^c-R_n^l)}\Delta S_n \quad (2)$$

The distance between the objects source and InSAR antennas ${R_n}^c$ and ${R_n}^l$ will be processed accurately to establish a new G matrix, then rewrite Eq. (2) into the matrix form:

$$\mathbf{V}_{M\times 1}=\mathbf{G}_{M\times N}\mathbf{T}_{N\times 1} \quad (3)$$

$$G(m,n)=e^{j\pi\Delta R_{mn}/\lambda} \quad (4)$$

$$\Delta R_{mn}=\sqrt{(x_n-X_{ml})^2+(y_n-Y_{ml})+R^2}-\sqrt{(x_n-X_{mc})^2+(y_n-Y_{mc})+R^2} \quad (5)$$

According to sparse representation theory and statistical information of natural images, natural image $x$ can be approximated to a sparse linear combination of the columns with a basis matrix $D$, therefore we can recover a sparse approximation $\hat{\theta}$ for $x$ by $D$, the basic model can be expressed as:

$$\hat{\theta_{ij}}=\arg\min_{\theta_{ij}}\sum_{ij}\left\|\theta_{ij}\right\|_0 \text{s.t.} D\cdot\theta=x \quad (6)$$

Therefore for object brightness temperature $T$ of InSAR, Eq. (3) will be rewritten to:

$$V_{M\times 1}=G_{M\times N}D^T_{N\times N}T'_{N\times 1} \quad (7)$$

Where $D_{N\times N}$ is an orthonormal basis constructed by discrete cosine transform. In the actual measurement of SAIR, $\varepsilon^2(V:T)$ is error functional and $E^2(T)$ is energy functional acting as an extra condition of convergence, reconstruction procedure of SAIR can be expressed as:

$$\min L_{\lambda_1,\lambda_2}(V:T)=\left\|\hat{\Phi}GD^TT'-\hat{V}\right\|_2+\lambda_1\left\|T'\right\|_1+\lambda_2\left\|T'\right\|_2 \quad (8)$$

Equation (8) is a minimization problem which largely depends upon the sparsity of InSAR images in transform domain and can be solved quickly by gradient iteration algorithms. Based on the above models, millimeter-wave InSAR imaging with sparse sensing can be considered as general holistic image processing, which short-circuits the need for segmentation, key-point matching, and other local operations caused by detail information-loss. However, the existing DCT in sparse InSAR imaging gives a promising method to detect salient object regions based on a bottom-up model.

## 3. A Spectrum-Based Saliency Detection Algorithm for Sparse InSAR

In this section, we combine and extend our previous work sparse InSAR imaging on spectral saliency detection [4]. Most importantly, we directly integrate the sparse InSAR imaging model and spectrum-based saliency detection model based on the existing of DCT. In recent years, beginning with the study by Hou and Zhang, spectrum-based saliency models attracted a lot of interest [5]. These approaches process the image's frequency spectrum based on fast Fourier transform to highlight sparse salient regions and provide state-of-the-art performance. However, what makes these approaches particularly attractive is the unusual combination of state-of-the-art performance and computational efficiency that is inherited from transform domain. As InSAR imaging is inverse Fourier transform procedure from visibility function, the DCT is adapted by sparse InSAR to ensure convergence condition. This letter is inspired by [6], which is based on DCT spectrum. We begin considering InSAR image $T$ which exhibits the following structure:

$$T=D^TT'=f_T+b_T+n,\quad f_T,b_T,n\in R^N \quad (9)$$

Where $f_T$ represents the foreground, $b_T$ represents the background and $n$ is imaging noise and error. As InSAR image is sparse in DCT domain, $f_T$ and $b_T$ is also sparsely supported in the basis of the DCT domain, that means they have only a small number of nonzero components. For the problem of figure-ground separation, we are only interested in the spatial support of $f_T$ ($f_T{}'$, the set of pixels for which $f_T$ is nonzero), where we have:

$$f_T=D^Tf_T{}' \quad (10)$$

According to the bottom-up model of human visual attention, $f_T{}'$ is the key component for saliency detection which is also difficult to be obtained directly. An alternative method is approximately isolating $f_T{}'$ by taking the sign of the mixture signal in the in the DCT domain and then do Inverse Discrete Cosine Transform (IDCT) to transform it back into the spatial domain. The new sparse representation is defined as imaging signature in [6]:

$$\bar{f}_T=IDCT[sign(T')] \quad (11)$$

Equation (11) is based on Uniform Uncertainty Principle (UUP) proposed by Candes and Tao [7], where we have:

$$E\left(\frac{<IDCT[sign(f_T')],IDCT[sign(T')]>}{\left\|IDCT[sign(f_T')]\right\|\bullet\left\|IDCT[sign(T')]\right\|}\right)\ge 0.5 \quad for\quad \Omega_b<\frac{N}{6} \quad (12)$$

Where, $\Omega_b$ is the number of nonzero pixels in the DCT domain of the background $b_T$ while $N$ is number of all background pixels. This constraint condition of sparsity is easy to be satisfied for InSAR images according to statistical information. Here $E$ function is the probability which means that Eq. (12) guarantees the validity of our methods. An important note is that Eq. (12) also means Eq. (11) does not

**Table 1** SSDA algorithm.

| |
|---|
| **Input:** $\hat{\Phi}$, $\hat{V}$, $\lambda_1$, $\lambda_2$, $N$ |
| **Output:** saliency map $m$ and highlighted reconstruction image. |
| **Algorithm:** |
| Step 1: calculate $\hat{\Phi} \cdot G \cdot D^T$ according to Eq. (4) and Eq. (5); |
| Step 2: initialize Eq. (8) and update it to get $T'$; |
| Step 3: calculate $\hat{f}_T$ by using Eq. (10); |
| Step 4: calculate saliency map $m$ by using Eq. (11) and Eq. (13); |
| Step 5: calculate highlighted reconstruction image by using $m$ and $T = D^T \cdot T'$ |

depend on the local relative energies of the foreground and background, only their sparseness in DCT domain, which means above operation is still holistic processing.

If we assume that an image foreground is a visually conspicuous object relative to its background, then we can form a saliency map $m$ by smoothing the squared reconstructed image defined above:

$$m = g * (\bar{f}_T \circ \bar{f}_T) \tag{13}$$

Where g is a Gaussian kernel and symbol $\circ$ represents Hadamard product operator. Spectrum-based saliency detection algorithm for millimeter-wave InSAR imaging with sparse sensing which will be referred to as SSDA is summarized in Table 1.

## 4. Simulations and Results

In the previous section, we established a theoretical model of the spectrum-based saliency detection algorithm for sparse millimeter-wave InSAR imaging. In this section, we will demonstrate the performance of the SSDA and give the image and numerical comparison with other saliency detection algorithms after InSAR accomplishing imaging with different system conditions.

For traditional InSAR imaging method, MFFT and G matrix need entire visibility function samples while CS method could just use part of the data [8], and the original Itti-Koch saliency model (denoted Itti) [9] will start detecting only after imaging accomplished.

In the first experiment, we compare the highlighted images generated by SSDA and other algorithms using a 64×64 real object brightness temperature distribution image of a plane shown in Fig. 1. The gray value of Fig. 1 represents the intensity of radiation sources at the frequency of 34GHz with 200MHz system bandwidth. For the foreground or the targets in Fig. 1, they are natural objects which are smooth and sparse in transformed domain.

The experimental result is shown in Fig. 2, which demonstrates SSDA performs a better visually saliency evaluation than others. Also, an important phenomenon is for the small point radiation source in the top left corner of the original image, SSDA shows strong ability to detect it while others do not, which results from the information-loss accused by InSAR imaging procedure and SSDA does not depend on the local relative energies which is guaranteed by Eq. (12). Also, improved by Eq. (13), for the point radiation source part SSDA produces smoother and better evaluation of target location.

**Fig. 1** Original scene: 34GHz object brightness temperature distribution of a plane

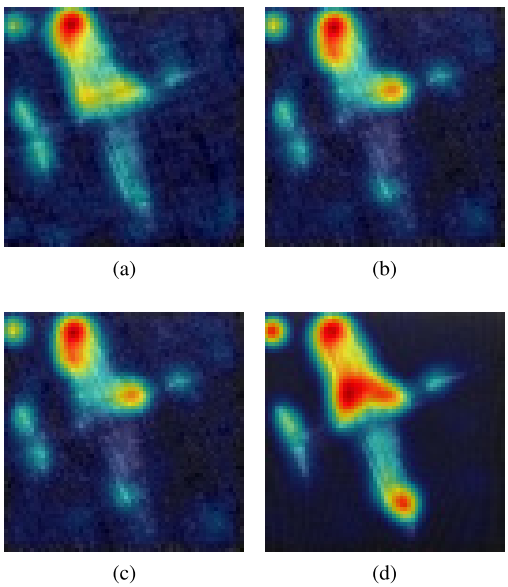


**Fig. 2** Highlighted reconstruction images. (a), (b), (c), (d) are generated by MFFT with Itti, G matrix with Itti, CS with Itti using 60% visibility function samples, SSDA using 60% visibility function samples, respectively.

In second experiments, the performance of CS with Itti and SSDA is evaluated by different usage percentage of visibility samples. Figure 3 shows saliency maps generated by CS with Itti and SSDA using 60% and 70% visibility function samples, from which we could see SSDA still performs a better visually saliency evaluation than CS with Itti.

Importantly, SSDA also runs faster than all competitors in our tests of computational performance, which results from that SSDA demands low computational cost by using part of the samples and could achieve detecting while imaging. Table 2 reports algorithm's Matlab runtime (on a PC with 3.6G Intel i7 processor, 16G memory) at different usage percentage of samples (undersampling rate).

Additionally, in real InSAR imaging, due to the errors in correlation observations and the receiving noise, InSAR images suffer from noise pollution. As SSDA adopts both error and energy functional, it performs better denoising ability than CS with Itti, which is shown in Fig. 4.

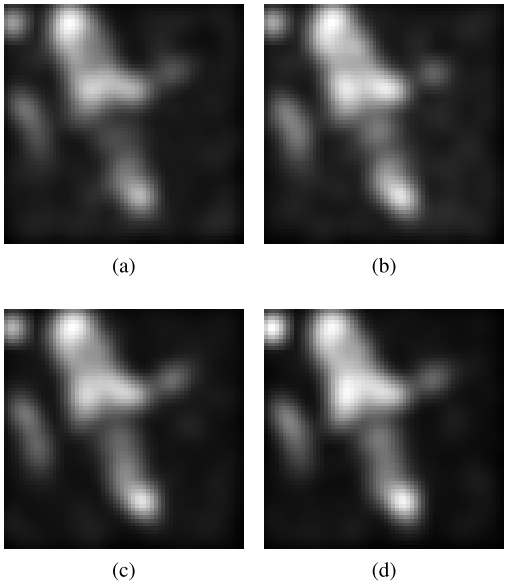

**Fig. 3** Saliency maps. (a), (b) are generated by CS with Itti using 60% and 70% visibility function samples, respectively; (c), (d) are generated by SSDA using 60% and 70% visibility function samples, respectively.

**Table 2** Average time cost(s) of CS with Itti and SSDA

| undersampling rate | 30% | 40% | 50% | 60% | 70% |
|---|---|---|---|---|---|
| CS wtih Itti | 18.45 | 22.53 | 24.98 | 65.87 | 150.43 |
| SSDA | 15.63 | 18.67 | 21.98 | 59.36 | 142.24 |

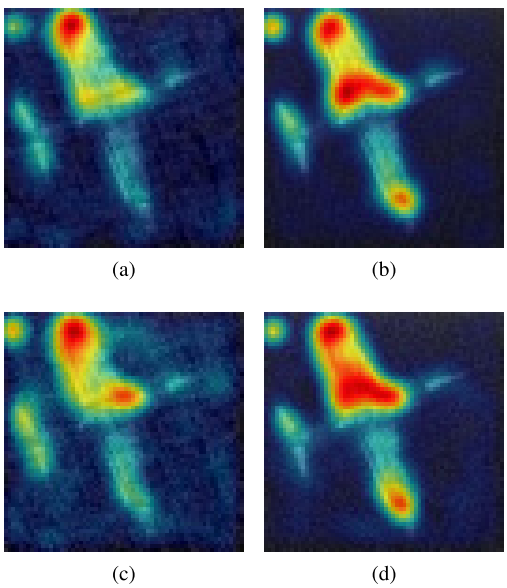

**Fig. 4** Highlighted reconstruction images. (a), (b) are generated by CS with Itti, SSDA using 60 % samples while Gaussian deviation is 0.1, respectively. (c), (d) are generated by CS with Itti, SSDA using 70 % samples while Gaussian deviation is 0.12, respectively.

## 5. Conclusion

In this letter, we have proposed a spectrum-based saliency detection algorithm, called SSDA, to extract the salient object regions from unknown backgrounds cooperating with sparse sensing InSAR imaging procedure. Directly using part of visibility function samples and sparse information of scenes in the basis of DCT domain, the proposed algorithm isolates the support of saliency region and then inversely transforms it back to calculate the saliency map. Experimental results show that SSDA provides better saliency evaluation at a lower data level and performs better of denoising compared to other detecting algorithms. Future work adopting high-quality image segmentation after spectrum-based saliency detecting is being developed.

## Acknowledgements

The authors would like to thank the anonymous reviewer and editors for their helpful comments and suggestions. This work is supported by the National Natural Science Foundation of China under Grants 60901008 and 61001010, National Ministry Foundation of China under Grants 51305050102, University Science Research Project of Jiangsu Province under Grants 15KJB510008.

### References

[1] L. Yujiri, M. Shoucri, and P. Moffa, "Passive millimeter wave imaging," IEEE Microw. Mag., vol.4, no.3, pp.39–50, Sept. 2003.

[2] H. Yang, F. Hu, K. Chen, D. Li, G. Yi, and R. Jin, "A robust regularization kernel regression algorithm for passive millimeter wave imaging target detection," IEEE Trans. Geosci. Remote Sen. Lett., vol.9, no.5, pp.915–919, Sept. 2012.

[3] M. Cheng, N.J. Mitra, X. Huang, P.H.S. Torr, and S.-M. Hu, "Global contrast based salient region detection," IEEE Trans. Pattern Anal. Mach. Intell., vol.37, no.3, pp.569–582, March 2015.

[4] Y. Zhang, Y. Li, G. He, and S. Zhang, "A compressive regularization imaging algorithm for millimeter-wave SAIR," IEICE Trans. Inf. Syst., vol.E98-D, no.8, pp.1609–1612, Aug. 2015.

[5] X. Hou and L. Zhang, "Saliency detection: A spectral residual approach," Proc. IEEE Conf. Computer Vision and Pattern Recognition, pp.1–8, June 2007.

[6] X. Hou, J. Harel, and C. Koch, "Image signature: Highlighting sparse salient regions," IEEE Trans. Pattern Anal. Mach. Intell., vol.34, no.1, pp.194–201, Jan. 2012.

[7] E. Candes and T. Tao, "Near-optimal signal recovery from random projections: Universal encoding strategies?," IEEE Trans. Inf. Theo., vol.52, no.12, pp.5406–5425, Dec. 2006.

[8] J. Chen and Y. Li, "The CS-Based imaging algorithm for near-Field synthetic aperture imaging radiometer," IEICE Trans. Electron., vol.E97-C, no.9, pp.911–914, Sept. 2014.

[9] L. Itti, C. Koch, and E. Niebur, "A model of saliency-based visual attention for rapid scene analysis," IEEE Trans. Pattern Anal. Mach. Intell., vol.20, no.11, pp.1254–1259, Nov. 1998.